



Valence change and local structure during cycling of layer-structured cathode materials

Pei-Yun Liao^a, Jenq-Gong Duh^{a,*}, Jyh-Fu Lee^b

^a Department of Materials Science and Engineering, National Tsing Hua University, Hsinchu, Taiwan

^b National Synchrotron Radiation Research Center, Hsinchu Science-Based Industrial Park, Hsinchu, Taiwan

ARTICLE INFO

Article history:

Received 19 June 2008

Received in revised form

25 December 2008

Accepted 31 December 2008

Available online 29 January 2009

Keywords:

Li-ion battery

Cathode

XAFS

XANES

ABSTRACT

Layer-structured Li-Ni-based oxide has been studied extensively as the promising cathode material for lithium ion battery because of its lower cost and higher practice capacity compared with the currently used LiCoO₂. In this study, the wide solid solutions of Mg-doped LiNi_{0.6-y}Mg_yCo_{0.25}Mn_{0.15}O₂ ($0 \leq y \leq 0.08$) with the layered α -NaFeO₂ structure were synthesized by the mixing hydroxide method. The capacity retention of LiNi_{0.57}Mg_{0.03}Co_{0.25}Mn_{0.15}O₂ in both room temperature and 55 °C was increased to 93%. The oxidation state and local environment of transition metals (Ni, Co and Mn) were studied by the high energy synchrotron X-ray absorption spectroscopy (XAS). The X-ray absorption near edge structure (XANES) indicated that the initial valences were 2+/3+, 3+ and 4+ for Ni, Co, and Mn, respectively, in the pristine LiNi_{0.57}Mg_{0.03}Co_{0.25}Mn_{0.15}O₂. The in situ XAS study with the cell charge to 5.2 V showed that the main redox reaction during delithiation was achieved by Ni (i.e. Ni²⁺/Ni³⁺ → Ni⁴⁺). The EXAFS data also exhibited that the bond length of Ni–O decreased drastically, while the Co–O and Mn–O distances exhibited a slight change with the decrease of Li content in the electrode. It was further revealed that all the second shell metal–metal (Ni–M, Co–M, and Mn–O) distances decreased due to the oxidation of metal ions and the contraction in *a*-axes of this structure.

© 2009 Elsevier B.V. All rights reserved.

1. Introduction

Rechargeable Li-ion batteries with the high energy density have become the most used power sources for a variety of portable electronic devices since the first commercialization of the battery in 1991 by Sony. Recently, layer-structured Li-Ni-based oxides have been investigated extensively because of their lower cost and higher practice capacity as compared with the currently used LiCoO₂ cathode. Among them, LiNi_{1-x}Co_xMn_yO₂ materials are reported to be the most attractive ones [1–4]. They provide a satisfied capacities and the good cycleability [3,4]. However, there are still safety and resistance concerns.

In literatures, many attempts have been made to improve the performance of cathode materials [5–8]. Cationic substitution for nickel to form substituted LiNi_{1-x}M_xO₂ (M = Fe, Mg, Al and Ti) could stabilize the Ni-based oxide and appeared to be a good method to modify the structural and electrochemical performance [5,9–12]. In a recent work, Mg-doped LiNi_{0.57}Mg_{0.03}Co_{0.25}Mn_{0.15}O₂ exhibited the good capacity retention. A small amount Mg substitution for Ni could stabilize the structure and make the phase transition from H1

to H2 completely during cycling test [13]. The thermal stability was also improved with the exothermic temperature rising from 209 to 250 °C.

In this work, the phase and electrochemical performance at high temperature for a series Mg-doped LiNi_{0.6-y}Mg_yCo_{0.25}Mn_{0.15}O₂ ($y=0, 0.01, 0.03, 0.05$ and 0.08) materials were investigated to obtain the optimum Mg substitution concentration. Recently, extensive researches on the electronic structure have been carried out with X-ray absorption spectroscopy (XAS). The changes of electronic transitions and local structure at Mn, Co and Ni K-edge for LiNi_{1/3}Co_{1/3}Mn_{1/3}O₂ were examined by XAS and only Ni atom was electroactive upon cycling [14–16]. For another layer-structured cathode, LiNi_{0.5}Mn_{0.5}O₂, it was found that the charge compensation was achieved mainly by the two step oxidation of Ni²⁺ (Ni²⁺ to Ni³⁺ first and then Ni³⁺ to Ni⁴⁺), while the manganese ion remained unchanged in Mn⁴⁺ oxidation state [17,18]. Especially, in situ X-ray absorption spectroscopy is a powerful tool to observe the changes during electrochemical reaction. Therefore, in this study the environments around Ni, Co and Mn ions for un-doped and Mg-doped LiNi_{0.6-y}Mg_yCo_{0.25}Mn_{0.15}O₂ were also observed by the X-ray absorption spectroscopy technique to discuss the mechanism of charge compensation during delithiation to high voltage 5.2V in the cathode materials.

* Corresponding author. Tel.: +886 3 5712686; fax: +886 3 5712686.

E-mail address: jgd@mx.nthu.edu.tw (J.-G. Duh).

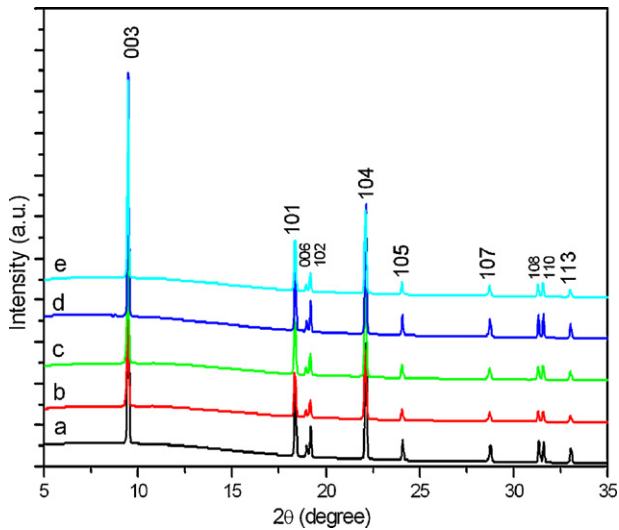


Fig. 1. XRD patterns of $\text{LiNi}_{0.6-y}\text{Mg}_y\text{Co}_{0.25}\text{Mn}_{0.15}\text{O}_2$ as a function of Mg doping amount for (a) $y=0$, (b) $y=0.01$, (c) $y=0.03$, (d) $y=0.05$, and (e) $y=0.08$ ($\lambda=0.7749 \text{ \AA}$).

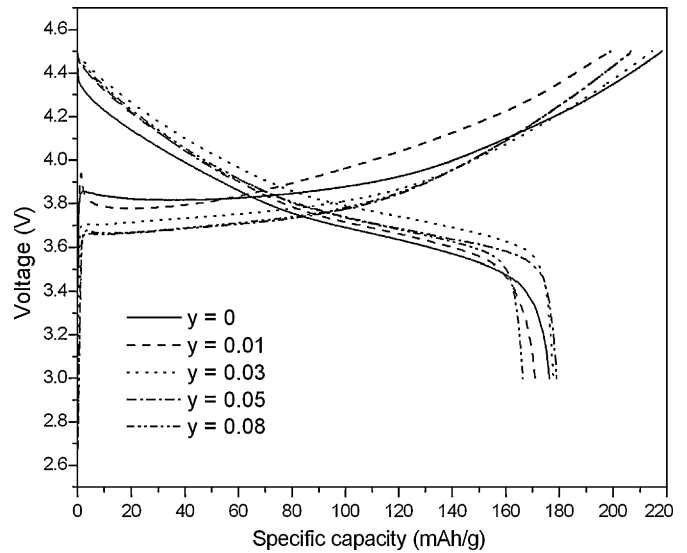


Fig. 3. The first charge/discharge curve of $\text{Li}/\text{LiNi}_{0.6-y}\text{Mg}_y\text{Co}_{0.25}\text{Mn}_{0.15}\text{O}_2$ cells.

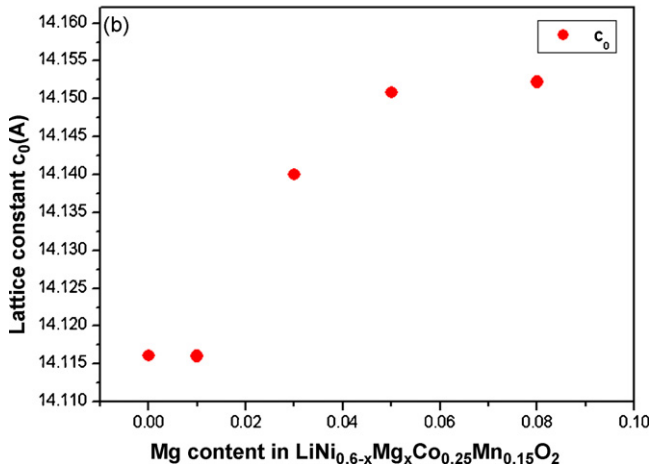
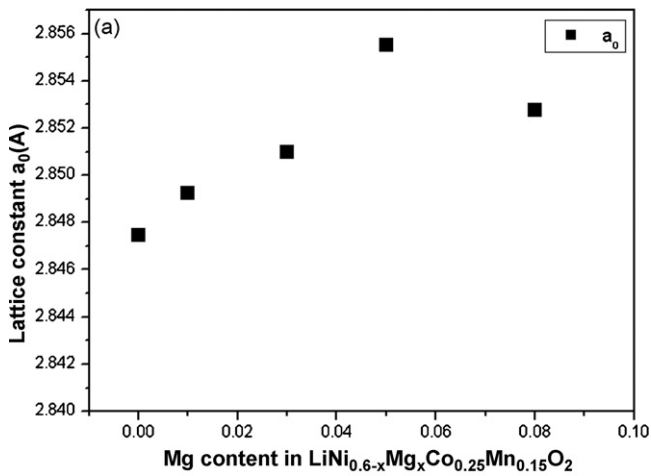


Fig. 2. (a) Lattice constant a and (b) lattice constant c as a function of Mg contents for $\text{LiNi}_{0.6-y}\text{Mg}_y\text{Co}_{0.25}\text{Mn}_{0.15}\text{O}_2$.

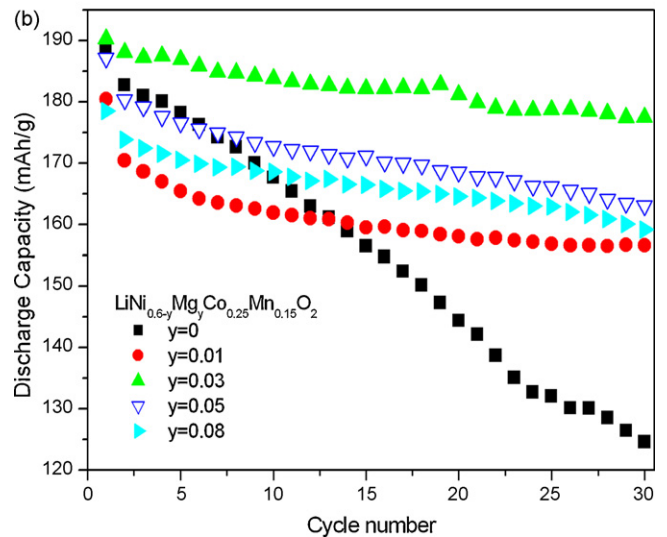
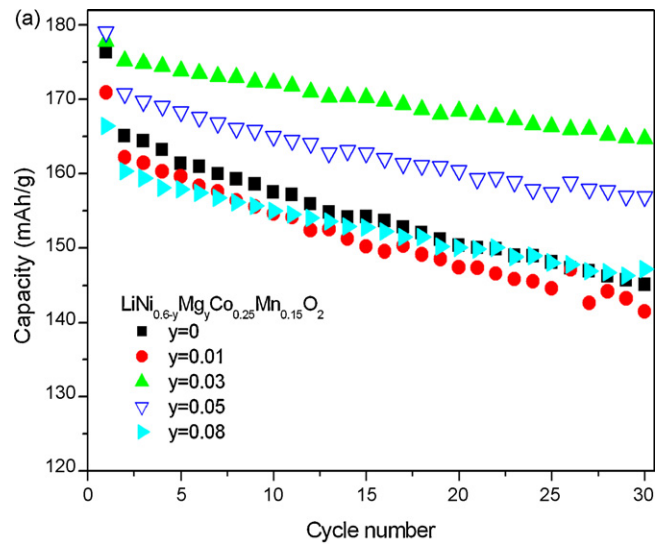


Fig. 4. Discharge capacity as a function of cycle number at (a) room temperature and (b) 55°C for $\text{LiNi}_{0.6-y}\text{Mg}_y\text{Co}_{0.25}\text{Mn}_{0.15}\text{O}_2$ ($y=0, 0.01, 0.03, 0.05$ and 0.08) in the voltage range 3–4.5 V.

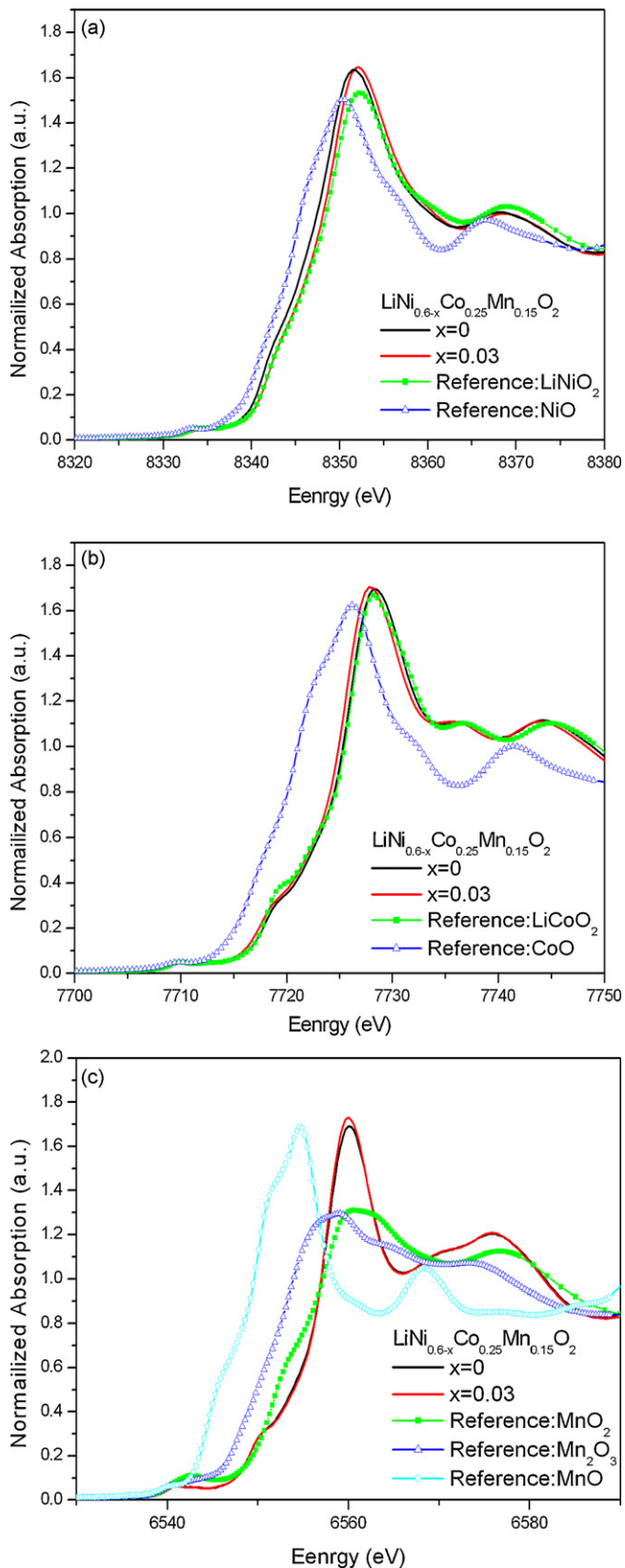


Fig. 5. Normalized XANES spectra of (a) Ni K-edge, (b) Co K-edge and (c) Mn K-edge for pristine $\text{LiNi}_{0.6}\text{Co}_{0.25}\text{Mn}_{0.15}\text{O}_2$ and Mg-doped $\text{LiNi}_{0.57}\text{Mg}_{0.03}\text{Co}_{0.25}\text{Mn}_{0.15}\text{O}_2$.

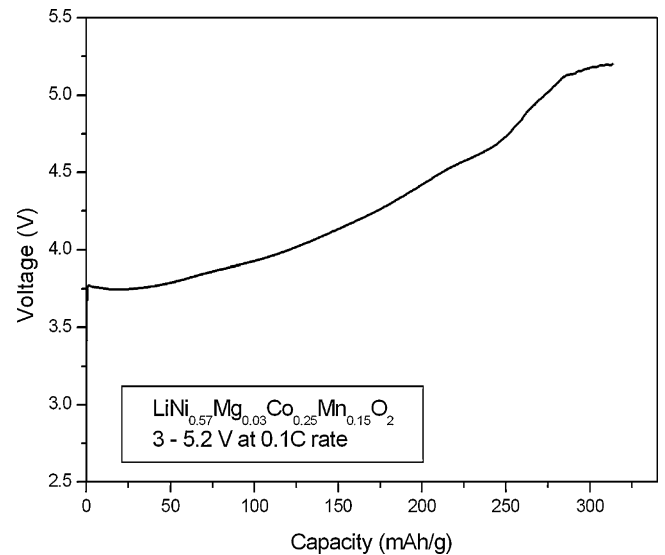


Fig. 6. The first charge curve for the in situ $\text{LiNi}_{0.57}\text{Mg}_{0.03}\text{Co}_{0.25}\text{Mn}_{0.15}\text{O}_2$ cell from 3 to 5.2 V at C/10 rate.

2. Experimental

The layered $\text{LiNi}_{0.6-y}\text{Mg}_y\text{Co}_{0.25}\text{Mn}_{0.15}\text{O}_2$ ($y = 0, 0.01, 0.03, 0.05$ and 0.08) compounds were synthesized by the mixing hydroxide method. The aqueous solution of $\text{NiSO}_4 \cdot 6\text{H}_2\text{O}$, $\text{CoSO}_4 \cdot 7\text{H}_2\text{O}$, MnSO_4 and MgSO_4 was slowly pumped into the reactor, meanwhile the aqueous solutions of NH_4OH and NaOH were also fed into the solution at a constant rate to adjust the pH value at 12. The filtrated precipitate was washed several times to ensure that the residual ions (Na^+ , SO_4^{2-} or others) were almost removed. The $[\text{Ni}_{0.6-y}\text{Mg}_y\text{Co}_{0.25}\text{Mn}_{0.15}\text{O}_2](\text{OH})_2$ product was dried, then mixed with Li_2CO_3 in ethanol using a mortar and pestle, and heated to 900°C for 15 h in the flowing O_2 to obtain $\text{LiNi}_{0.6-y}\text{Mg}_y\text{Co}_{0.25}\text{Mn}_{0.15}\text{O}_2$ ($y = 0, 0.01, 0.03, 0.05$ and 0.08) powders.

The phase identification of prepared powders was carried out in the transmission mode at 16 keV ($\lambda = 0.7749 \text{ \AA}$) in the National Synchrotron Radiation Research Center (NSRRC, Taiwan). The exposure time was 3 min and XRD spectra were recorded on the Mar 345-image plate detector.

The electrodes were fabricated with a mixture of 89 wt.% cathode powder, 2 wt.% super P, 4 wt.% KS6, and 5 wt.% polyvinylidene difluoride (PVDF) binder in N-methyl-2-pyrrolidone (NMP) to obtain a slurry. 1 M LiPF_6 in a 1:2 (volume ratio) mixture of EC/DMC was used as the electrolyte. Type 2016 coin-cells (20 mm in diameter and 1.6 mm thick) were assembled with the Li foil as an anode in an argon glove box where both moisture and oxygen content were < 1 ppm. The cells were cycled at C/5 current rate in the voltage range of 3–4.5 V at room temperature and 55°C .

The cell designation of in situ XRD experiments was similar to the regular one for the electrochemical test. To have in situ X-ray pass through the cathode electrode, holes with 4ϕ were drilled in the upper cover, bottom cover and Ni spacer of the 2016 coin-cell and followed by sealing with a Kapton film. In situ XAS experiments of metal K-edge were performed in transmission mode at beam line BL-17C in the National Synchrotron Radiation Research Center (NSRRC, Taiwan). The energy selection was actualized by a Si (1 1 1) double crystal monochromator. The metal foil (Ni, Co and Mn) was employed for energy calibration in each scan simultaneously. To analyze the in situ XAS data, all raw absorption spectra were normalized to compare the regions of pre-edge, near-edge and post-edge. For extended X-ray absorption fine structure (EXAFS)

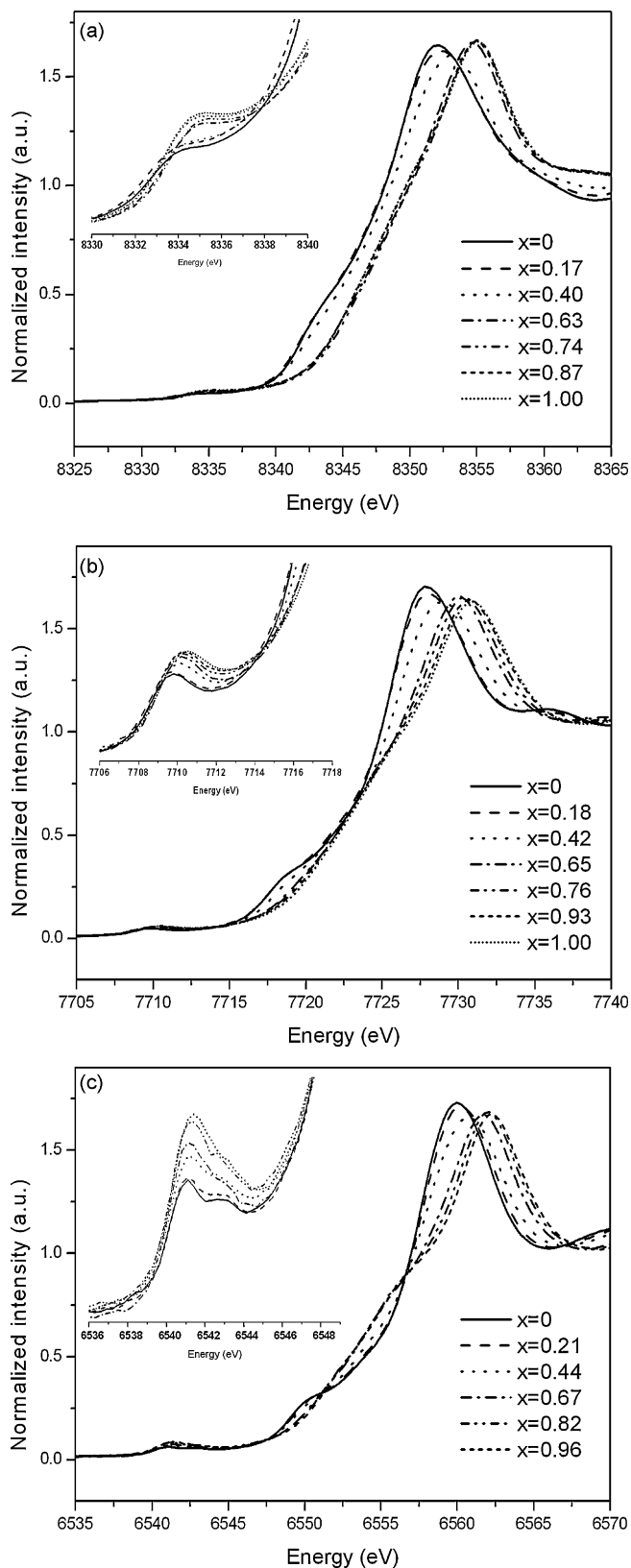


Fig. 7. Normalized (a) Ni K-edge, (b) Co K-edge, and (c) Mn K-edge XANES spectra for $\text{Li}_{1-x}\text{Ni}_{0.57}\text{Mg}_{0.03}\text{Co}_{0.25}\text{Mn}_{0.15}\text{O}_2$ as a function of lithium content x during charged to 5.2 V. The insets show the pre-edge feature of the respective XAS spectra.

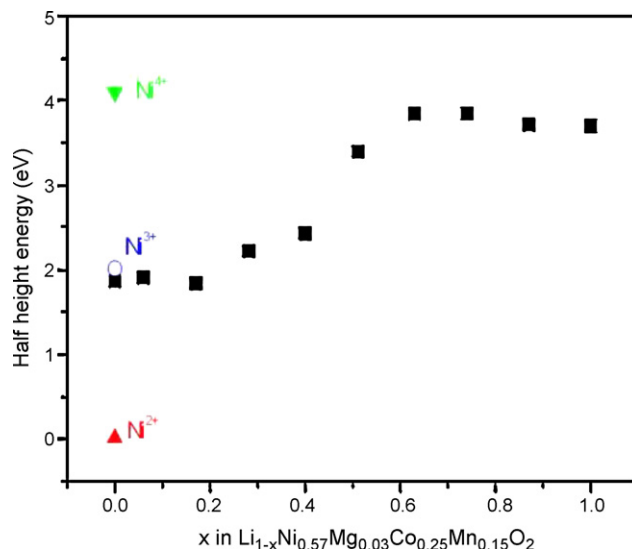


Fig. 8. Energy shifts of Ni K-edge at the half-height energy for $\text{Li}_{1-x}\text{Ni}_{0.57}\text{Mg}_{0.03}\text{Co}_{0.25}\text{Mn}_{0.15}\text{O}_2$ as a function of lithium content x during charged to 5.2 V.

spectra, pre-edge background was subtracted, and then normalized with respect to the edge jump. The normalized $\chi(E)$ spectra were converted to $\chi(k)$ in k space. The k^3 -weighted $\chi(k)$ data ranged from 3.55 to 13.65 \AA^{-1} for Ni K-edge, 3.65 to 12.1 \AA^{-1} for Co K-edge, and 3.7 to 12 \AA^{-1} for Mn K-edge were Fourier transformed (FT) to r space by separating the EXAFS contributions according to different coordination shells. EXAFS structural parameters were obtained by nonlinear least-squares analysis using phase and amplitude functions generated by FEFF7 code. All fitting procedure and parameters including the coordination number (N) and the Debye–Waller factor were executed by the UWXAFS 3.0 software package.

3. Results and discussion

The X-ray diffraction patterns of the $\text{LiNi}_{0.6-y}\text{Mg}_y\text{Co}_{0.25}\text{Mn}_{0.15}\text{O}_2$ ($y = 0, 0.01, 0.03, 0.05$ and 0.08) for various Mg substitution amounts are shown in Fig. 1. All the peaks can be indexed based on a hexagonal $\alpha\text{-NaFeO}_2$ structure (space group: $R\bar{3}m$, No. 166) in which oxygen ions are in a close-packed FCC array and Li and transition metal ions occupy the 3a and 3b octahedral sites, respectively, on the alternate (1 1 1) plane. Doping does not change the structure and no impurity phases can be observed. Fig. 2(a) and (b) shows the changes of lattice constants a and c , respectively, as the function of Mg content. As the Mg substitution increases, lattice constants of $\text{LiNi}_{0.6-y}\text{Mg}_y\text{Co}_{0.25}\text{Mn}_{0.15}\text{O}_2$ increase, which is attributed to the larger radius of Mg^{2+} ion ($r_{\text{Mg}^{2+}} = 0.72 \text{ \AA}$, $r_{\text{Ni}^{2+}} = 0.72 \text{ \AA}$ and $r_{\text{Ni}^{3+}} = 0.56 \text{ \AA}$), indicating that a solid solution in the range of $0 \leq y \leq 0.08$ for $\text{LiNi}_{0.6-y}\text{Mg}_y\text{Co}_{0.25}\text{Mn}_{0.15}\text{O}_2$ is formed. In addition, the obvious splits of (006, 102) and (108, 110) couples suggest an ordering layered structure for these materials.

Fig. 3 shows the first charge-discharge profiles of $\text{Li}/\text{LiNi}_{0.6-y}\text{Mg}_y\text{Co}_{0.25}\text{Mn}_{0.15}\text{O}_2$ ($y = 0, 0.01, 0.03, 0.05$ and 0.08) cells in the potential range 3–4.5 V cycled at 0.2 C current rate. The $\text{Li}/\text{LiNi}_{0.6-y}\text{Mg}_y\text{Co}_{0.25}\text{Mn}_{0.15}\text{O}_2$ cells exhibit smooth and monotonous voltage curves and the plateaus of charge decrease slightly with Mg substitution. The large irreversible capacity of the first cycle was mainly due to the SEI formation [19] and the incomplete reduction of Ni^{4+} ions [14]. Fig. 4 shows the discharge capacity at both room temperature and 55 °C as a function of cycle number. The increase of initial capacity at 55 °C is attributed to the higher

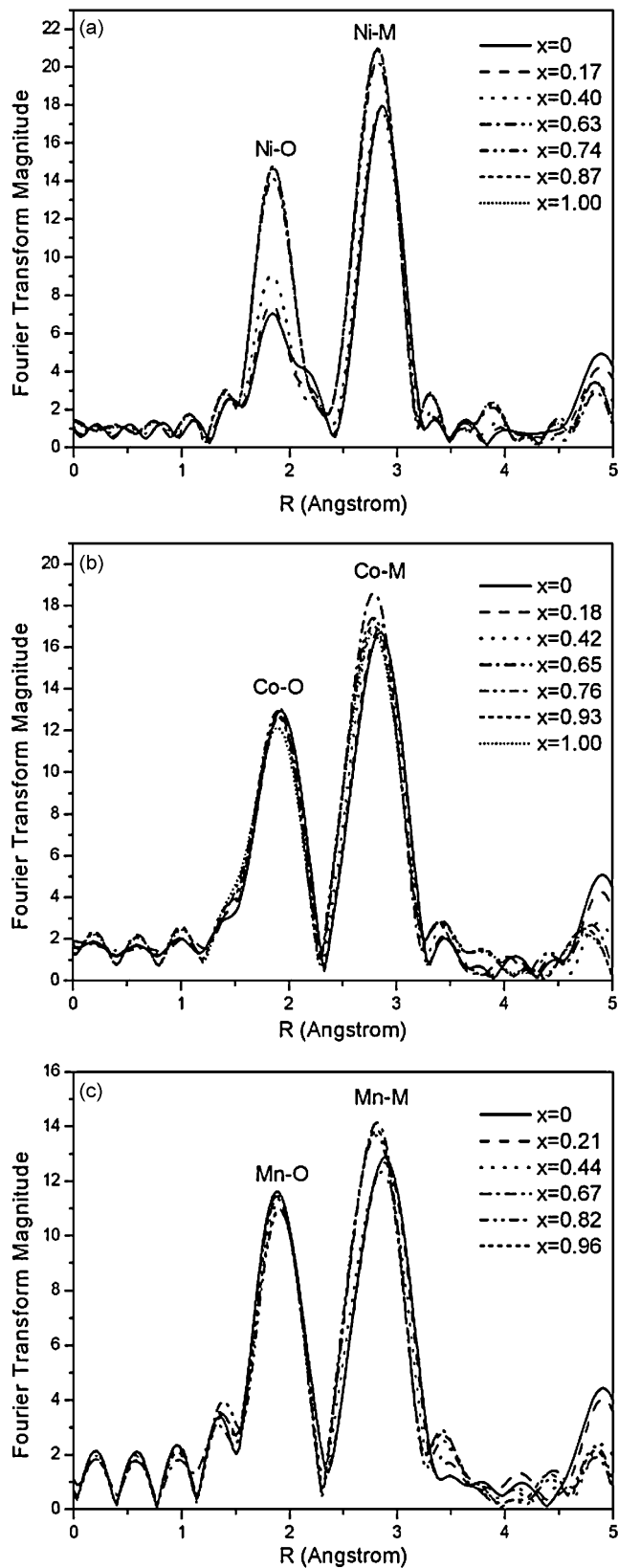


Fig. 9. Fourier transformed spectra of the (a) Ni K-edge, (b) Co K-edge, and (c) Mn K-edge for $\text{Li}_{1-x}\text{Ni}_{0.57}\text{Mg}_{0.03}\text{Co}_{0.25}\text{Mn}_{0.15}\text{O}_2$ as a function of lithium content x during charged to 5.2 V.

mobility of Li ions. It appears that a small amount of addition Mg in $\text{LiNi}_{0.6-y}\text{Mg}_y\text{Co}_{0.25}\text{Mn}_{0.15}\text{O}_2$ can improve the cycling performance, especially the capacity retention at high temperature. In both cases, the sample with $y=0.03$ exhibits the best electrochemical performance. The initial capacity of $\text{LiNi}_{0.57}\text{Mg}_{0.03}\text{Co}_{0.25}\text{Mn}_{0.15}\text{O}_2$ is 214 mAh g^{-1} and has an excellent cyclic performance with only 7% capacity loss after 30 cycles at both temperatures.

Meanwhile, the valence of transition metal ions for $\text{LiNi}_{0.6-y}\text{Mg}_y\text{Co}_{0.25}\text{Mn}_{0.15}\text{O}_2$ sample is studied by the X-ray absorption spectroscopy technique. Fig. 5 shows the normalized Ni, Co, and Mn K-edge X-ray absorption near edge structure (XANES) spectra for pristine $\text{LiNi}_{0.6}\text{Co}_{0.25}\text{Mn}_{0.15}\text{O}_2$ and $\text{LiNi}_{0.57}\text{Mg}_{0.03}\text{Co}_{0.25}\text{Mn}_{0.15}\text{O}_2$ powders with their reference compounds. The XANES analysis provides a deep insight into the oxidation state and local environment of the absorber atoms. The Ni K-edge spectrum in Fig. 5(a) reveals that in comparison with pristine $\text{LiNi}_{0.6}\text{Co}_{0.25}\text{Mn}_{0.15}\text{O}_2$, a slight edge shift to high energy is observed in the Mg-doped $\text{LiNi}_{0.57}\text{Mg}_{0.03}\text{Co}_{0.25}\text{Mn}_{0.15}\text{O}_2$. A previous XPS study showed that valence of Ni was a mixture of 2+ and 3+ for $\text{LiNi}_{0.6}\text{Co}_{0.25}\text{Mn}_{0.15}\text{O}_2$ [4]. This indicates that the oxidation state of Ni increases with the substitution of Mg^{2+} ions. In contrast, there is no apparent shift in Co and Mn K-edge XANES spectra, implying that their valences are not affected by the Mg doping. The oxidation states for Co and Mn are 3+ and 4+, respectively, in both $\text{LiNi}_{0.6}\text{Co}_{0.25}\text{Mn}_{0.15}\text{O}_2$ and $\text{LiNi}_{0.57}\text{Mg}_{0.03}\text{Co}_{0.25}\text{Mn}_{0.15}\text{O}_2$ samples.

Fig. 6 shows the voltage profile of the in situ $\text{Li}/\text{LiNi}_{0.57}\text{Mg}_{0.03}\text{Co}_{0.25}\text{Mn}_{0.15}\text{O}_2$ cell charged at the current rate of $C/10$ (0.288 mA) to 5.2 V. In order to extract all lithium ions out of the host structure and to further study the structural change, the cut-off voltage was set higher than the normal one. The calculated capacity at 5.2 V was around 313 mAh g^{-1} , which was larger than the theoretical one of 275 mAh g^{-1} due to the decomposition of electrolyte at the high voltage. Fig. 7 shows the in situ Ni, Co, and Mn K-edge XANES spectra for $\text{Li}_{1-x}\text{Ni}_{0.57}\text{Mg}_{0.03}\text{Co}_{0.25}\text{Mn}_{0.15}\text{O}_2$ cathode material as a function of x . The value of x is calculated from the specific capacity divided by the theoretical one. The chemical shift in the metal K-edge spectra has a correlation with the oxidation states of the absorber atoms. As x increases from $x=0$ to $x=0.63$ in Fig. 7(a), the Ni K-edge energy continuously shifts to higher energy, indicating the increasing oxidation state of Ni. The energy shift at the half-step height used as an indicator of oxidation state of active Ni is plotted with Li contents in Fig. 8. As compared with the reference compounds, it is clearly seen that the nickel valence in the pristine $\text{LiNi}_{0.57}\text{Mg}_{0.03}\text{Co}_{0.25}\text{Mn}_{0.15}\text{O}_2$ before charge is a mixture of Ni^{2+} and Ni^{3+} . As expected, the valence of Ni continuously increases in the range of $0 < x < 0.63$. The oxidation process of nickel ions compensates the charge during delithiation and provides the capacity. With further deintercalation of lithium ions from $x=0.63$ to $x=1$ in the higher voltage, there is no more shift in the energy of Ni K-edge XANES, suggesting that Ni^{2+} and Ni^{3+} are fully oxidized to Ni^{4+} .

For Co K-edge spectrum, it is noted that the variation in Fig. 7(b) has a different trend as compared with Ni K-edge. It shows an obvious shape change of the Co absorption spectrum, indicating that Li-intercalation causes the change in electronic structure of Co atoms [20–22]. It was found that the charge compensation for Li-deintercalation was closely associated with the rehybridization of Co and O orbitals [20,23]. The previous calculation showed that $\text{Co}^{3+}/\text{Co}^{4+}$ redox reaction would occur in the range of $2/3 \leq x \leq 1$ for $\text{Li}_{1-x}\text{Ni}_{1/3}\text{Co}_{1/3}\text{Mn}_{1/3}\text{O}_2$ [24]. In this work, the small energy shift is observed in the pre-edge region for Co K-edge XANES, demonstrating that $\text{Co}^{3+}/\text{Co}^{4+}$ oxidation reaction occurs during delithiation. Besides, it is supposed that part of charge compensation in high voltage range (4.7–5.2 V) is also achieved via the oxidation of electrolyte. In the case of Mn K-edge XANES shown

Table 1
Structural parameters from the curve fitting results for Ni K-edge EXAFS of $\text{Li}_{1-x}\text{Ni}_{0.57}\text{Mg}_{0.03}\text{Co}_{0.25}\text{Mn}_{0.15}\text{O}_2$ during charge: CN is the coordination number at this distance and σ^2 is the Debye–Waller factor.

x in Li_{1-x}	Ni–O CN	Ni–O distance (Å)	σ^2 (10^{-3})	Ni–M CN	Ni–M distance (Å)	σ^2 (10^{-3})	R-factor
0.00	6	1.952	8.25	6	2.865	4.43	0.005865
0.06	6	1.938	8.16	6	2.861	4.44	0.005175
0.17	6	1.922	7.91	6	2.856	4.47	0.004337
0.28	6	1.910	7.36	6	2.851	4.52	0.004662
0.40	6	1.896	6.31	6	2.841	4.55	0.004714
0.51	6	1.880	4.28	6	2.821	4.36	0.002374
0.63	6	1.885	3.08	6	2.812	3.76	0.003421
0.74	6	1.885	2.89	6	2.813	3.59	0.002637
0.87	6	1.885	2.88	6	2.814	3.57	0.002866
1.00	6	1.886	2.93	6	2.816	3.57	0.003141

Table 2
Structural parameters from the curve fitting results for Co K-edge EXAFS of $\text{Li}_{1-x}\text{Ni}_{0.57}\text{Mg}_{0.03}\text{Co}_{0.25}\text{Mn}_{0.15}\text{O}_2$ during charge: CN is the coordination number at this distance and σ^2 is the Debye–Waller factor.

x in Li_{1-x}	Co–O CN	Co–O distance (Å)	σ^2 (10^{-3})	Co–M CN	Co–M distance (Å)	σ^2 (10^{-3})	R-factor
0.00	6	1.926	3.17	6	2.857	3.83	0.003052
0.08	6	1.923	3.24	6	2.852	3.84	0.002732
0.18	6	1.923	3.33	6	2.849	3.82	0.003988
0.30	6	1.918	3.28	6	2.843	3.77	0.003724
0.42	6	1.912	3.33	6	2.833	3.68	0.003575
0.54	6	1.901	3.44	6	2.814	3.39	0.004507
0.65	6	1.896	3.58	6	2.813	3.32	0.005074
0.76	6	1.890	3.57	6	2.815	3.42	0.005124
0.93	6	1.888	3.65	6	2.819	3.50	0.006143
1.00	6	1.884	3.90	6	2.821	3.63	0.008438

Table 3
Structural parameters from the curve fitting results for Mn K-edge EXAFS of $\text{Li}_{1-x}\text{Ni}_{0.57}\text{Mg}_{0.03}\text{Co}_{0.25}\text{Mn}_{0.15}\text{O}_2$ during charge: CN is the coordination number at this distance and σ^2 is the Debye–Waller factor.

x in Li_{1-x}	Mn–O CN	Mn–O distance (Å)	σ^2 (10^{-3})	Mn–M CN	Mn–M distance (Å)	σ^2 (10^{-3})	R-factor
0.00	6	1.919	3.86	6	2.874	5.87	0.017673
0.10	6	1.918	3.86	6	2.871	5.86	0.017207
0.21	6	1.918	4.07	6	2.866	6.06	0.017927
0.32	6	1.916	4.04	6	2.855	5.88	0.016798
0.44	6	1.913	4.34	6	2.845	6.30	0.014802
0.56	6	1.909	4.44	6	2.821	5.91	0.013723
0.67	6	1.906	4.13	6	2.820	5.59	0.010836
0.70	6	1.909	4.26	6	2.818	5.57	0.015606
0.82	6	1.912	4.62	6	2.817	5.67	0.012817
0.96	6	1.913	4.45	6	2.820	5.59	0.015956

in Fig. 7(c), some shape changes show up without a rigid peak shift, indicating that the local environment around Mn ions is altered during charge. Actually, oxidation state of Mn in the pristine $\text{LiNi}_{0.57}\text{Mg}_{0.03}\text{Co}_{0.25}\text{Mn}_{0.15}\text{O}_2$ powder is already 4+, and would not be oxidized further with Li deintercalation. The role of inactive Mn^{4+} ions in layer-structured cathode materials, such as $\text{Li}_{1-x}\text{Ni}_{1/3}\text{Co}_{1/3}\text{Mn}_{1/3}\text{O}_2$ and $\text{Li}_{1-x}\text{Ni}_{1/2}\text{Mn}_{1/2}\text{O}_2$, is always to stabilize the structure [24–27].

Fig. 9 shows the Fourier transform magnitudes for Ni, Co and Mn K-edge EXAFS spectra during charge. The first peak at around 1.9 Å is attributed to the six nearest neighboring oxygens around Ni, Co and Mn absorbers. The second peak at 2.8 Å is assigned to the six-coordinated transition metal Ni/Co/Mn ions around the absorber atom in transition metal layer. It is revealed that on delithiation Ni–O distance varies dramatically, while the changes for Co–O and Mn–O distances are rather negligible. The reason is that the charge compensation mainly occurs at the Ni sites, resulting in a significant decrease in the average Ni–O distance. Besides, the peak amplitude of Ni–O and Ni–M bonds in the Ni K-edge EXAFS spectrum increases upon charge. According to previous studies [28,29], Ni^{3+} exhibited Jahn–Teller distortion with contributions from 4 O atoms

in the shorter distance of 1.92 Å and 2 O atoms in the long distance of 2.06 Å, while Ni^{4+} had a regular octahedral coordination with 6 O atoms at 1.88 Å. Therefore, the increase in peak amplitude is due to the decrease of Jahn–Teller Ni^{3+} ions during the deintercalation of Li ions.

The structural parameters obtained by fitting the first two peaks of FT spectra are listed in Tables 1–3 for Ni, Co and Mn K-edge EXAFS, respectively. All the values of R-factor for the fitting data are smaller than 0.02, indicating a good fitting and consistency with the model. At the pristine state, bond lengths are 1.95, 1.93 and 1.92 Å for Ni–O, Co–O and Mn–O, respectively. The bond length of Ni–O is between 2.05 Å for Ni^{2+} –O and 1.93 Å for Ni^{3+} –O [14], which again confirming the coexistence of Ni^{2+} and Ni^{3+} in $\text{LiNi}_{0.57}\text{Mg}_{0.03}\text{Co}_{0.25}\text{Mn}_{0.15}\text{O}_2$. During delithiation, the dramatic decreases in Ni–O and Ni–M bond distances are observed. The first shell Ni–O length decreases to 1.88 Å for the end compound $\text{Ni}_{0.57}\text{Mg}_{0.03}\text{Co}_{0.25}\text{Mn}_{0.15}\text{O}_2$, which is consistent with the calculated Ni^{4+} –O bond length [24]. From these tables, it clearly demonstrates that the variation in Mn–O distance is the least (only 0.01 Å), while that of the Ni–O distance is the largest, i.e. 0.07 Å during the whole charge process. In contrast, the change of the second shell metal to metal (Ni–M, Co–M and

Mn–O) distances almost varies by 0.05 Å between the initial and fully charge state. The bond distances of Ni–M, Co–M and Mn–M decrease upon charging, which correspond to the contraction of lattice constant “*a*” on the transition metal plane of this structure [30].

4. Conclusions

LiNi_{0.6–y}Mg_yCo_{0.25}Mn_{0.15}O₂ (*y* = 0, 0.01, 0.03, 0.05 and 0.08) were synthesized by the mixing hydroxide method. Mg substitution did not change the phase and no impurity was observed, indicating that a homogeneous solid solution could exist in the range of 0 ≤ *y* ≤ 0.08 for LiNi_{0.6–y}Mg_yCo_{0.25}Mn_{0.15}O₂. The capacity retention was highly improved by the Mg dopant, especially in the high temperature of 55 °C. LiNi_{0.57}Mg_{0.03}Co_{0.25}Mn_{0.15}O₂ exhibited an excellent cyclic performance with 93% retention after 30 cycles. The XANES data demonstrated that Mg substitution could only change the valence of Ni. The initial oxidation states for Ni, Co and Mn are 2+/3+, 3+, and 4+, respectively. During charge, the main charge compensation occurred by the oxidation of Ni and Co ions, and the peak amplitude in the Fourier transformed spectra of Ni K-edge increased owing to the decrease of Jahn-Teller ion Ni³⁺. In contrast, valences of Mn⁴⁺ remained unchanged even at 5.2 V. In the high voltage, the charge compensation was achieved not only by the oxidation of Co³⁺ but also by the side reaction of electrolyte.

Acknowledgments

The authors are grateful to National Science Council, Taiwan (No. NSC 96-2221-E-007-093) for the partial financial support. We also thank the group of Dr. Jyh-Fu Lee for their technical assistance and the National Synchrotron Radiation Research Center (NRSSC) for the use of synchrotron X-ray diffraction facilities.

References

[1] T. Ohzuku, Y. Makimura, Chem. Lett. (2001) 642.

- [2] S.H. Park, C.S. Yoon, S.G. Kang, H.S. Kim, S.I. Moon, Y.K. Sun, Electrochim. Acta 49 (2004) 557.
- [3] N. Yabuuchi, T. Ohzuku, J. Power Sources 119–121 (2003) 171.
- [4] P.Y. Liao, J.G. Duh, S.R. Sheen, J. Electrochem. Soc. 152 (9) (2005) A1695.
- [5] C. Poullierie, L. Croguennec, Ph. Biendan, P. Willmann, C. Delmas, J. Electrochem. Soc. 147 (6) (2000) 2061.
- [6] S.B. Jang, S.H. Kang, K. Amine, Y.C. Bar, Y.K. Sun, Electrochim. Acta 50 (2005) 4168.
- [7] K.S. Lee, S.T. Myung, H.J. Bang, S. Chung, Y.K. Sun, Electrochim. Acta 52 (2007) 5201.
- [8] H.W. Chan, J.G. Duh, J.F. Lee, Electrochem. Commun. 8 (2006) 1731.
- [9] R. Kanno, T. Shirane, Y. Inaba, Y. Kawamoto, J. Power Sources 68 (1997) 145.
- [10] T. Ohzuku, A. Ueda, M. Kouguchi, J. Electrochem. Soc. 142 (1995) 4033.
- [11] W.S. Yoon, K.Y. Chung, M. McBreen, X.Q. Yang, Electrochem. Commun. 8 (2006) 1257.
- [12] C.C. Chang, J.Y. Kim, P.N. Kumta, J. Electrochem. Soc. 147 (5) (2000) 1722.
- [13] P.Y. Liao, J.G. Duh, H.S. Sheu, J. Power Sources 183 (2008) 766.
- [14] Y.W. Tsai, B.J. Hwang, G. Ceder, H.S. Sheu, D.G. Liu, J.F. Lee, Chem. Mater. 17 (2005) 3191.
- [15] T. Nedoseykina, S. Kim, Y. Nitta, Electrochim. Acta 52 (2006) 1467.
- [16] A. Deb, U. Bergmann, S.P. Cramer, E.J. Cairns, J. Appl. Phys. 97 (2005) 113523.
- [17] W.S. Yoon, M. Balasubramanian, X.Q. Yang, J. McBreen, Z. Fu, D.A. Fischer, J. McBreen, J. Electrochem. Soc. 151 (2004) A246.
- [18] Y. Arachi, H. Kobayashi, S. Emura, Y. Nakata, M. Tanaka, T. Asai, H. Sakaebe, K. Tatsumi, H. Kageyama, Solid State Ionics 176 (2005) 895.
- [19] Z. Wang, Y. Sun, L. Chen, X. Huang, J. Electrochem. Soc. 151 (2004) A914.
- [20] C.H. Chen, B.J. Hwang, C.Y. Chen, S.K. Hu, J.M. Chen, H.S. Sheu, J.F. Lee, J. Power Sources 174 (2007) 938.
- [21] W.S. Yoon, M. Balasubramanian, K.Y. Chung, X.Q. Yang, J. McBreen, C.P. Grey, F.A. Fischer, J. Am. Chem. Soc. 127 (2005) 17479.
- [22] C.S. Johnson, A.J. Kropf, Electrochim. Acta 47 (2002) 3187.
- [23] W.S. Yoon, C.P. Grey, M. Balasubramanian, X.Q. Yang, D.A. Fischer, J. McBreen, Electrochem. Solid-State Lett. 7 (2004) A53.
- [24] Y. Koyama, N. Yabuuchi, I. Tanaka, H. Adachi, T. Ohzuku, J. Electrochem. Soc. 151 (2004) A1545.
- [25] A. Deb, E.J. Cairns, Fluid Phase Equilibria 241 (2006) 4.
- [26] A. Deb, U. Bergmann, S.P. Cramer, E.J. Cairns, J. Appl. Phys. 99 (2006) 063701.
- [27] W.S. Yoon, C.P. Grey, M. Balasubramanian, X.Q. Yang, J. McBreen, Chem. Mater. 15 (2003) 3161.
- [28] A.N. Mansour, X.Q. Yang, X. Sun, J. McBreen, L. Croguennec, C. Delmas, J. Electrochem. Soc. 147 (2000) 2104.
- [29] I. Nakai, K. Takahashi, Y. Shiraishi, T. Nakagome, F. Izumi, Y. Ishii, F. Nishikawa, T. Konishi, J. Power Sources 68 (1997) 536.
- [30] P.Y. Liao, J.G. Duh, J.F. Lee, H.S. Sheu, Electrochim. Acta 53 (2007) 1850.